# Liesegang Rings, Pattern Formation at Phase Transition; Experiments and Mathematical Modelling.

Michiel Hazewinkel, C.W.I. Amsterdam.
Johan F. Kaashoek, Econometric Inst., Erasmus Univ. Rotterdam.
Bart Leynse, Dept. Chem. Path., Erasmus Univ. Rotterdam.

Abstract.

Liesegang rings are periodic precipitation patterns. In this paper three mathematical models on phase transition are reviewed and confronted with observations obtained from Liesegang experiments. Two of the models, the competitive particle growth model and the autocatalytic growth model were proposed earlier. In the third model, called the anti-diffusion model, pattern formation is generated by a mass transport process. This mechanism is consistent with a mass conservating phase transition. Existence of bounded, non constant solutions will be shown.

## I. Introduction.

One of the best known periodic precipitation phenomena was discovered in 1896 by Liesegang [8] and named for the discoverer. Many compounds are capable of producing Liesegang rings or bands when subjected to the proper conditions. In our experiments we used OH diffusing into a gel containing cobaltouschloride. After some hours the first ring is produced. The ring consists of microscopically small crystals of $Co[OH]_2$. The resulting patterns bear a strong resemblance to magmatic crystallization [9].

Already in 1897 Wi Ostwald [11] presented an explanation of the Liesegang phenomena in terms of supersaturation and diffusion. Ostwald's theory was of qualitative nature only. Mathematical treatments of Ostwald's supersaturation theory were forwarded in former times by Prager [13]. They treated diffusion but not analyse the chemical reaction and precipitation. Therefore, they were not able to calcultate the sizes and time of formation of the rings. Recently Keller and Rubinow [6] presented a mathematical formulation of Wi Ostwald's supersaturation theory. Not only diffusion but also the chemical reaction and the precipitation of the product are considered.

Flicker and Ross [3] have chosen another approach. They postulate colloid formation preceding the precipitation and autocatalytic particle growth induced by increasing ion concentration within the electric double layer with increasing colloid concentration. In consequence Flicker and Ross propose a mechanism based on chemical instability for the explanation of periodic precipitation phenomena. The mathematical model is of reaction-diffusion type. They mention the work of Turing [14] and Prigogine et all [10] on symmetry breaking instability. Flicker and Ross critisized the Ostwald theory because it does not predict revertspacing of the rings nor secondary structures and requires an imposed concentration gradient. In their opinion supersaturation is unnecessary for periodicity; diffusion of the precipitate must be taken in account. Their system consists of

fast and slow diffusing substances which, with a non-linear reaction scheme, can produce periodic patterns [1].

In a second type of experiments a uniform sol of the precipitate is allowed to age. Spatially inhomogeneous structures arise but this process is slow and it can takes days for the larger particles to grow substantially at the cost of smaller ones. These experiments are strongly related to the evolution of a secondary structure in ordinary Liesegang experiments, called secondary banding: one bands breaks up into a sequence of more closely spaced bands. Since both these phenomena occur only after coarsening or riping of the sol, they must be placed in the cadre of crystal growth and dissolution. The model after Ortoleva [2] called competitive particle growth model, has the formal structure of interaction between a diffusible substance and a non-diffusible variable representing the radius of large particles. It is based on the principle discovered by Wī Ostwald [12] and names for him, Ostwald's ripining.

Although in the models of Flicker and Ross and Ortoleva [2] diffusion generates structure, instability is caused by the reaction mechanism. However the Liesegang phenomenon is typically a form of molecular aggregation with a mass flux from low concentration areas to high concentration areas. Such a dynamic behavior will enlarge the fluctuations present in a chemical system and can easily induce pattern formation. Apparently these fluxes are opposed to the classical Fickian diffusion flux and the aggregating transient behavior can be characterized by a negative diffusion coefficient [1]. The model we shall propose will be a three component system and the pattern generating behavior will depend on a competition between a clustering mechanism for the Co -component and dissolution and precipitation of the $Co[OH]_2$ component. Clustering will be modelled by an so-called anti-diffusion term which means that in linear approximation for some homogeneous concentration level of $Co^{++}$, the diffusion can be negative. This anti-diffusion term is derived in [5] and the basic form is similar to a generalized diffusion equation based on the

Landau-Ginzburg free energy model where in the onset of phase separation the diffusion is negative [1]. Since in the experiments is observed that ringformation depends on the environmental variable pH, the clustering mechanisme in our model will depend on the $OH^-$ concentration. The dissolution and precipitation will be approximated by a simple stable chemical reaction mechanism.

This rapport is organized as follows. In section II some Liesegang experiments are reported. A reaction-diffusion model after Flicker and Ross and the competitive particle growth model are reviewed in section III.1, resp. section III.2. In section III.3 we shall introduce the anti-diffusion model. For uniform equilibrium solutions of the three models a linear stability analysis is performed. Numerical solutions of the models are also reported in the relevant sections.

## II. The Liesegang Experiment.

### II.1 Experiments and theoretical considerations.

The experimental results here reported are taken from the work of L. Zwang, Dept. Chem. Path. Erasmus Univ. Rotterdam. The following experimental setup is chosen : a tube is divided in three successive zones: one with an initial cobalt concentration of 50 mmol/l (Co-zone), one with respect to Co and OH, neutral zone (NZ-zone), one with an initial OH concentration between 0.1 and 1.0 mol/l (OH-zone). See figure 2.1.


Figure 2.1 Liesegang experiment setup.

This configuration is denoted as (OH-NZ-Co, a-b-c) where a,b and c are respectivily the lenght of the zones in mm. The overall medium is an Agar-Agar 1% concentrate.

The very characteristics of the transient behavior in a Liesegang experiment is clearly seen by contrasting experiments with $NH_4Cl$ and ones without. For an (OH-NZ-Co,10-15-25) configuration, table 1 gives the results of an experiment with $NH_4Cl$ (overall initial concentration 0.15 mol/l) and table 2 gives the results without $NH_4Cl$.The reported Co concentration is measured by taking intersections k, k=1,2,3.. at different locations $x_k$, k=1,2,3.., always ordered such that $x_i$ is closer to the OH-zone then $x_j$ if $i < j$.

In both experiments is found that in the neighbourhood of the Co-NZ boundary (table 1, intersection 9; table 2, intersection 10), the germ of a ring is formed. At the intersections 10, resp. 9, Co becomes more concentrated then in neighbouring locations by attracting Co ions. In all these experiments a pH of approximately 8.5 was a necessary condition of germ-formation. But the $NH_4Cl$-and

the non-$NH_4Cl$ experiment differ completely in further evolution.

| no. intersection | $[Co^{++}]$ (mmol/l) |
|---|---|
| 1 | 0 |
| 2 | 0 |
| 3 | 0 |
| 4 | 0 |
| 5 | 1 |
| 6 | 2 |
| 7 | 1 |
| 8 | 34 |
| 9 | 49 |
| 10 | 54 |
| 11 | 35 |
| 12 | 33 |
| 13 | 45 |
| 14 | 55 |
| 15 | 58 |

table 1. Experiment with $NH_4Cl$.

| no. intersection | $[Co^{++}]$ (mmol/l) |
|---|---|
| 1 | 0 |
| 2 | 0 |
| 3 | 0 |
| 4 | 3 |
| 5 | 5 |
| 6 | 9 |
| 7 | 14 |
| 8 | 14 |
| 9 | 55 |
| 10 | 38 |
| 11 | 35 |
| 12 | 45 |
| 13 | 52 |
| 14 | 55 |
| 15 | 58 |

table 2. Experiment without $NH_4Cl$.

Whereas in the $NH_4Cl$ experiment precipitation of $Co[OH]_2$ occurs only after some 190 minutes, in the non-$NH_4Cl$ experiment precipitation starts already after 40 minutes. This means that in the first case the depletion of the neighbourhood of a germ location is lasting far longer then in the second case. So, in some distance of a germ, the precipitation saturation level can not be reached anymore. At longer distance the depletion will be less effective and the arise of a second germ becomes possible. Since depletion goes along with a growth of the germ, in due course the precipitation saturation level will be reached at such a location; finally a periodic precipitation pattern will be observed. In figure 2.2 a time evolution of a $NH_4Cl$ experiment is depicted. At time t=100 minutes the first ring is already clearly seen. The second ring at location 7.5 began to rise at time t=180 minutes. Observed was that ring one was still growing further when ring two began to rise. This observation contradicts the theory of Ostwald which stated that rings can only arise if the foregoing ring is completely formed and is not growing further [12].

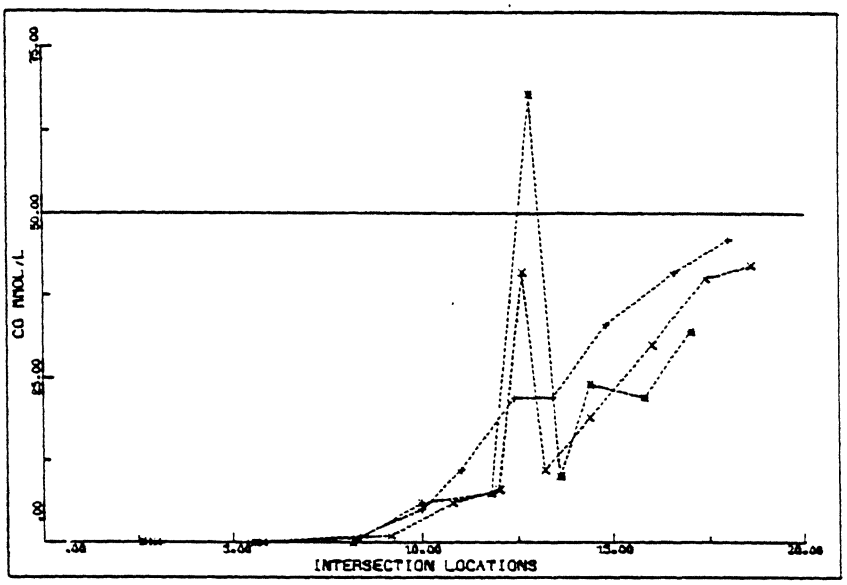


Figure 2.2: $Co^{++}$ concentration time evolution in a $NH_4CL$ experiment. +: 20 min., x: 100 min., *: 230 min..

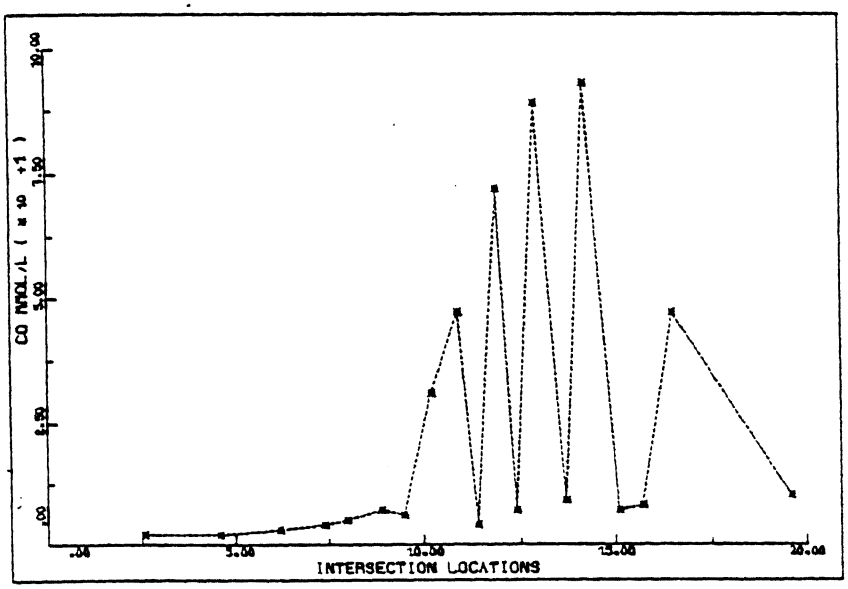


Figure 2.3: $Co^{++}$ concentration pattern in a $NH_4Cl$ experiment.

In figure 2.3 a more evolved Co pattern is shown. Note that the concentration in a ring becomes far more higher then the initial concentration of 50 mmol/l.

In the non-$NH_4Cl$ experiment sufficient depletion can not occur because of the fast precipitation. Consequently a continuous precipitate is formed. The depletion effect is a competition between large and small clusters of the $Co[OH]_2$ complex where just as in the case of crystal growth large clusters grow at the cost of smalles ones since larger ones are more stable then smaller ones. (See also section III and IV.)

The time delay of precipitation caused by $NH_4Cl$ is similar to the effect of some electrolytes on delaying or suppressing flocculation [7]. By submitting an electrolyte to the system the electric double layer of a $Co[OH]_2$ complex becomes more extended such that the probability that particles will lump together decreases. This competition between depletion and precipitation is also observed in the following experiments: as mentioned above, a pH - environment of 8.5 seems a necessary condition for ringforming with a relative low Co gradient. The time to get from a pH of 8.4 to a pH of 8.6 depends on the $NH_4Cl$ concentration present in the system. Table 3 gives the results for different $NH_4Cl$ concentrations with an Agar-Agar gel and with an AgaroseEF gel.

| | $[NH_4Cl]$ (mmol/l) | time (minutes) | observed pattern |
|---|---|---|---|
| Agar-Agar | 0 | 5 | continuous precipitate |
| | 150 | 11 | ring formation |
| | 400 | 20 | no precipitate at all |
| AgaroseEF | 0 | 8 | continuous precipitate |
| | 150 | 13 | continuous precipitate |
| | 400 | 17 | ring formation |
| | 800 | 30 | no precipiate at all |

Table 3. Time to get from pH 8.4 to 8.6 at different $NH_4Cl$ concentrations and the relation to precipitation.

The reported effects on ringformation are consistent. The high increase rate at low $NH_4Cl$ concentration is coupled with a fast precipitation rate of the $Co[OH]_2$ complex such that depletion effects are relatively small and not effective. If the increase rate is small, growth rate in neighbouring locations will differ only slightly. Then depletion conceived as competition between large and small clusters will not effective; a high $NH_4Cl$ concentration will prevent precipitation at all. The same effects are observed by varying the OH gradient. If too strong, the growth in pH is fast and only continuous precipitation occurs. If too low, even if a pH of 8.5 can be reached, the final state is a homogeneous one with no precipitation at all.

## II.2 Revert spacing and temperature.

In the above reported experiments a relatif strong OH gradient was imposed. This introduces a predominant direction in the system with as a consequence the observed spacing of the rings. In this case a Co gradient is not even necessary. (See also below). By making the Co gradient relatif strong with respect to the OH gradient, revert spacing is observed.

In a (OH-NZ-Co, 15-0-45) experiment with $[Co^{++}]$ 16 mmol/l and 5% $NH_4OH$ and a temperature of 23°C ringformation takes place after at least 30 hours. By submitting the same system to a watherbath of 37°C ringformation occurs after some few minutes. Table 4 gives the distance of the first ring to the OH-Co boundary in relation to the time at which the system is heated up to 37°C.

The above mentioned observations are combined in the following experiment. At low temperature, Co is homogeneously distributed and an OH concentrate is injected in the centre of the system. After some time which allows OH to diffuse, the system is heated up and a three dimensional spherical precipitation pattern is observed (Leynse Spheres). In this process no initial Co gradient is involved.

| no. | time T (minutes) | distance OH/Co (mm) |
|---|---|---|
| 1 | 14 | 2.90 |
| 2 | 31 | 4.80 |
| 3 | 54 | 6.20 |
| 4 | 87 | 8.05 |
| 5 | 129 | 10.05 |
| 6 | 157 | 11.24 |
| 7 | 184 | 12.00 |
| 8 | 207 | 12.79 |
| 9 | 241 | 13.65 |
| 10 | 275 | 14.34 |
| 11 | 308 | 14.80 |

Table 4. Ringformation and temperature. Initial temp. 23°C, after time T (see col. 2) temp. is 37°C; location of first ring is given in col. 3.

## II.3 Conclusions.

The Liesegang experiment is a system with multiple stationary states: homogeneous, continuous precipitate, periodic precipitate, no precipitate at all. The stability of a state in continuously tested by thermal fluctuations inherent to the system. Transition from one state to another will set in if some necessary conditions are fullfilled which means at least that the initial state becomes unstable. At sufficiently high OH-concentration locally germ formation of $Co[OH]_2$ clusters will start. This is a far from equilibrium process sustained by a mass flow towards the germ generating an autocatalytic groth effect on the germ and depletion effect on the neighbourhood. The strenght of these effects depends firstly on the initial deviations induced by thermal fluctuations and the imposed gradients of OH and Co. Secondly on the duration, that is the delay of precipiatation which is obtained by submitting an electrolyte to the system.

## III. Mathematical Models.

In this section we shall present and review three pattern formation models. The first one is an (autocatalytic) reaction-diffusion model due to Flicker and Ross [3]. The model is included as a representative of the plain reaction-diffusion models which are used in modelling pattern formation. The second is the so called competitive particle growth model which is based on Ostwald ripining. The final model, called anti-diffusion, describes the germformation as a local mass flow to maxima of the mass density.

### III.1. An Autocatalytic Growth Model.

#### III.1.1. Assumptions and model formulation.

Basically two processes are distinquished: the formation of colloid particles and an autocatalytic growth mechanism induced by electric double layer effects.

Assumptions:

i) The chemical process is of multistep type. Let colloid particles be formed of AB molecules. Assume that for $n \geq n^*$ aggregates $(AB)_n$ are more stable then $(AB)_{n-n_1}$, $n_1 = 1, \ldots, n-1, n$, then the multistep process is reduced to:

$$pA + qB \rightleftarrows (AB)_{n^*} \qquad \text{(III.1.1)}$$

(p,q integers, greater then one).
The complex $(AB)_{n^*}$ is denoted as C.

ii) As C is formed, it becomes charged by preferential adsorption of A or B. The primary charge is neutralized by a diffuse layer of counterions, ions with sign opposite to the primary layer ions. This is called the

electric double layer [7].

Processes in the primary layer are described as follows:

$$C + B \rightleftarrows C'$$
$$C + A \rightleftarrows C'' \qquad \text{(III.1.2)}$$

where primes denote colloid particles with different ionic environments. For simplicity the average concentration of all colloid particles is approximated by C, even is suggested to neglect (III.1.2) at all [3].

The essential autocatalytic growth process is argued by the notion that above a certain density of the colloid particles C, the product of the concentrations of A and B in the double layer is monotone increasing function in the C concentration [3]. So the probability to form C increases with increasing density of C. This autocatalytic effect of the double layer is approximated by a reaction mechanism :

$$r_1 C + p_1 A + q_1 B \rightleftarrows (1 + r_1)C \qquad \text{(III.1.3)}$$

where $r_1, p_1$ and $q_1$ are positive constants.

By assuming linear Fickian diffusion for each of the components A, B and C, the resulting mathematical model has the structure of pure reaction-diffusion equations.

Taking p=4, q=2, $p_1$=2, $q_1$=1 and $r_1$=3 and introducing scaling factors $A_0$, $B_0$, $C_0$, characteristic time and lenght, the evolution equations on an one-dimensional spatial domain $[0, I_o] \subset \mathbb{R}$ can be reduced to :

$$\frac{\partial \alpha}{\partial t} = D_\alpha \frac{\partial^2 \alpha}{\partial x^2} - (1 + \alpha)^4(1 + \beta)^2 - K_1(1 + \alpha)^2(1 + \beta)(1 + \gamma)^3 + \\ -K_2(1 + \alpha)(1 + \gamma) + K_3(1 + \gamma) \qquad \text{(III.1.4.1)}$$

$$\frac{\partial \beta}{\partial t} = D_\beta \frac{\partial^2 \beta}{\partial x^2} - \frac{1}{2}(1 + \alpha)^4(1 + \beta)^2 - \frac{1}{2}K_1(1 + \alpha)^2(1 + \beta)(1 + \gamma)^3 + \\ -K_2(1 + \beta)(1 + \gamma) + K_4(1 + \gamma) \qquad \text{(III.1.4.2)}$$

$$\frac{\partial \gamma}{\partial t} = D_\gamma \frac{\partial^2 \gamma}{\partial x^2} + (1+\alpha)^4(1+\beta)^2 + 2K_1(1+\alpha)^2(1+\beta)(1+\gamma)^3 + -K_5(1+\gamma) \qquad \text{(III.1.4.3)}$$

No flux boundary conditions are taken.
The dimensionless variables $\alpha$, $\beta$ and $\gamma$ are defined by $A = A_o(1+\alpha)$; $B = B_o(1+\beta)$ and $C = C_o(1+\gamma)$.
With respect to the model of Flicker and Ross, we have added a dissolution mechanism in the process of (III.1.1) ($K_3, K_4, K_5 \neq 0$) and made the reaction (III.1.3) cubic in $\gamma$. In this way the model can have multiple uniform equilibrium solutions whereas the original model does not allow for any uniform solution at all.

## III.1.2. Linear stability analysis.

The stability of an homogeneous solution $(A_o, B_o, C_o)$ is found by a linear stability analysis of the null solution $(\alpha,\beta,\gamma)=(0,0,0)$ of (III.1.4). The eigenvalues associated with the eigenvectors, proportional to $\cos(\frac{l\pi}{l_o}x)$, $l=1,2,\ldots$, decide on the stability of this null solution. For each l, we denote the largest eigenvalue by $\mu^+(l)$.

If $K_1 = 5$, $K_2 = 5$, $K_3 = 11$, $K_4 = 8$, $K_5 = 11$ and $D_\alpha = D_\beta = 10$ then for $D_\gamma = 0.01 * D_\alpha$, $\mu^+(l)$ is positive for $0 \leq l \leq 22$, with largest value at l=5. So, from the linear analysis, the development of a spatial structure can be expected if the null solution is disturbed. Since the coefficients of $\gamma$ in the linearized evolution equations of $\alpha$ and $\beta$ are negative, one could expect that $\alpha$ and $\beta$ are $180^o$ out of phase with $\gamma$ which will give some $\alpha$, $\beta$ -flux to local maxima of $\gamma$.

## III.1.3. Numerical simulations.

The pattern generating dynamics of autocatalytic reaction diffusion models are well known [10]. So we shall restrict us to one simulation with $D_\gamma = 0.01.D_\alpha$ and all other parameters as in

the foregoing section.

The initial evolution of a randomly disturbed null solution (homogeneous solution) is according to the linear stability analysis. However the final pattern is dominated by one growing centre. The autocatalytic growth in this centre is not sufficiently bounded by the dissolution process (third term in right hand side of equation (III.1.4.3)). Only depletion of the constituents $\alpha$ or $\beta$ will stop further growth. Note that $\alpha$ and $\gamma$ are indeed $180^{\circ}$ out of phase. See figure 3.1.

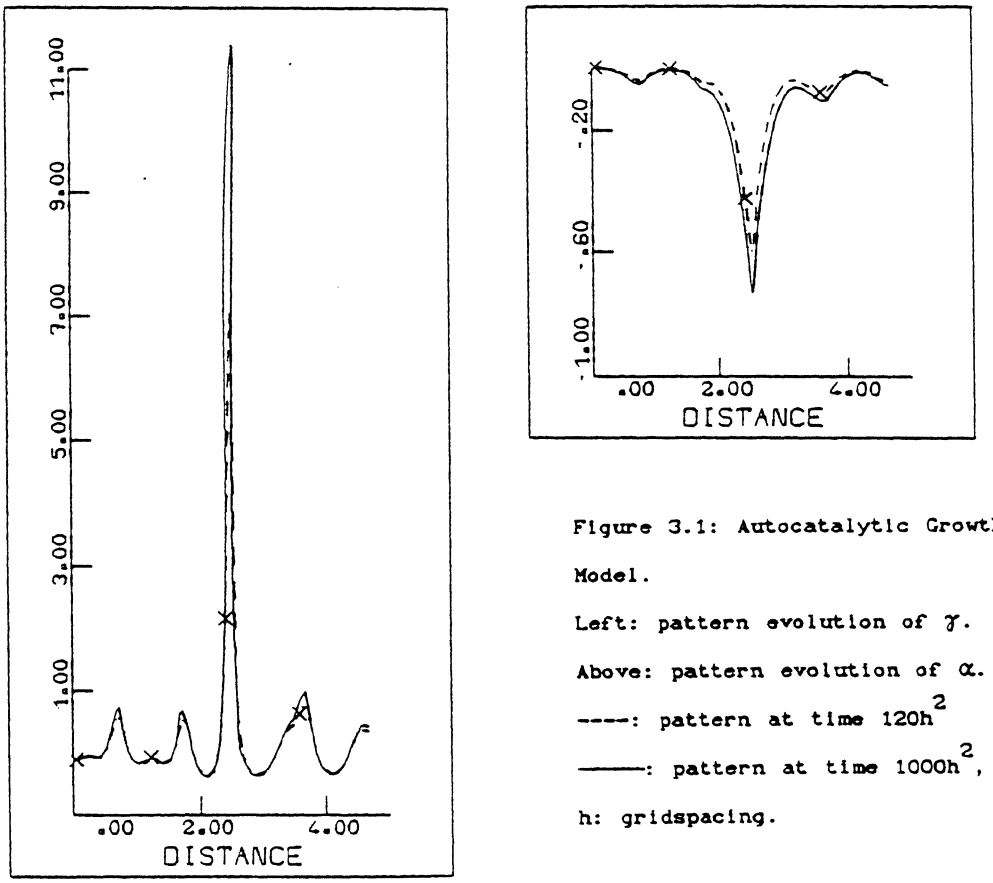


Figure 3.1: Autocatalytic Growth Model.

Left: pattern evolution of $\gamma$.

Above: pattern evolution of $\alpha$.

----: pattern at time $120h^2$

———: pattern at time $1000h^2$,

h: gridspacing.

III.1.4. Comment.

Essential in this model is the chemical reaction instability induced by the autocatalytic reaction scheme of (III.3). But is is not easily seen how the electric double layer will be the cause of a reaction instability. In contrast, for a uniform sol with constant environment, it is knowm that the electric double layer tends to stabilise the sol in the sense that no precipitation will occur. Just by reducing the effectivity of the electric double layer, that is by reducing his range, the sol can become unstable and molecular clumping can set in [7]. So arguing an autocatalytic growth which induces instability, on electric double layer effects, just contradicts the properties of this layer.

## III.2. Competitive Particle Growth Model.

An extensive review of the competitive particle growth model can be found in Feeney e.a. [2]. The model is based on interpedence of particle growth, diffusion and the precipitation particle dependence on the equilibrium concentration.

### III.2.1. Assumptions and model formulation.

The basic assumptions are:

i) a particle growth-dissolution process is restricted to : $P_n + P_1 \rightleftarrows P_{n+1}$
where $P_n$, n=1,2,.. is an aggregate of n monomers.

ii) at each point in space, the concentration $c_n$ of the polymers $P_n$ is and stays narrowly peaked about some $n^*(x,t)$. So, assuming spherical particles, in any small spatial domain the (large) particles are represented by a particle with radius R(x,t).

iii) surface free energy will cause that any large particle has an equilibrium monomer concentration $C^{eq}$. Assumed is that for large R, $C^{eq}(R)$ is monotonically decreasing in R. Then, for large R, a local maximum in R will grow and cause dissolution in its surroundings. In turn minima will induce secondary maxima in R.

The model is described in the monomer concentration C(x,t) and the local average particle size R(x,t). Changes in particle size are given by:

$$\frac{\partial R(x,t)}{\partial t} = \frac{K}{\rho}\left[ C(x,t) - C^{eq}(R)\right] \qquad \text{(III.2.1)}$$

where $\rho$ is molar density and K a reaction constant. Mass conservation leads to the following evolution equation for C:

$$\frac{\partial C(x,t)}{\partial t} = D\Delta C - n\rho\frac{\partial}{\partial t}(\tfrac{4}{3}\pi R^3) + \frac{qW}{\varepsilon} \qquad \text{(III.2.2)}$$

where n is number density of precipitate particles, assumed to be time independent, $D\Delta C$ diffusion according to Fick's Law ($D > 0$, constant) and $\frac{qW}{\varepsilon}$ is the source term of monomer production.
The equilibrium concentration $C^{eq}(R)$ is given by :

$$C^{eq}(R) = C^{eq}(\infty)\left[ 1 + \frac{2\Gamma R^2}{2R^3 + R_c^3}\right] \qquad \text{(III.2.3)}$$

with $C^{eq}(\infty)$: scaling parameter, $\Gamma$ a constant involving surface tension, crystal molar density, absolute temperature etc. and R: critical radius. Dimensionless variables are defined as follows :

$C = C^{eq}(1 + s)$; $R = \bar{R}\psi$; $x = \bar{L}\xi$; $t = \bar{t}\tau$; $n = \bar{n}\nu$ and $\sigma = \frac{\bar{R}}{\Gamma}s$,

where $\bar{}$ denotes characteristic values. This gives the following model:

$$\frac{\partial \psi}{\partial \tau} = \sigma - g(\psi,\psi_c) \qquad \text{(III.2.4.1)}$$

$$\frac{1}{\beta}\frac{\partial \sigma}{\partial \tau} = \Delta\sigma - \psi^2 \nu \frac{\partial \psi}{\partial \tau} + \frac{qW}{\varepsilon} \qquad \text{(III.2.4.2)}$$

$$g(\psi, \psi_c) = \frac{2\psi^2}{2\psi^3 + \psi_c^3} \qquad \text{(III.2.4.3)}$$

with no flux boundary conditions.
($\beta$ is dimensionless combination of $C^{eq}(\infty)$, $\Gamma$, $\bar{n}$ and $\bar{R}$ or equivalently of D, $\bar{L}$ and $\bar{t}$; $\psi_c = \frac{R_c}{R}$ ). In the following the source term $\frac{qW}{\varepsilon}$ is neglected and $\nu$ is set to 1.

III.2.2. Linear stability analysis.

Any uniform distribution of $\psi$ and $\sigma$ defined by $\psi(\xi,.) = \psi_o$, $\sigma(\xi,.) = \sigma_o$ with $\sigma_o = g(\psi_o, \psi_c)$ is a solution of (III.2.4).
Now consider the system on a closed interval $I = \{ \xi \in \mathbb{R} \mid 0 \leq \xi \leq I_o \}$ then a linear stability analysis shows that every uniform solution with $\left.\frac{dg}{d\psi}\right|_{\psi=\psi_c} < 0$ is unstable. The linear approximation of the right hand side of (III.2.4) defines a linear operator on the solution space $L^2[0,I]$. Then, given the no flux boundary conditions, eigenvectors are proportional to $\cos(\frac{l\pi\xi}{I})$ and the eigenvalues $\mu(l)$ must satisfy :

$$\mu^2(l) + \mu(l)\left[g_1 + \beta p^2 + \beta\psi_o^2\right] + \beta g_1 p^2 = 0$$

where $g_1 = \left.\frac{dg}{d\psi}\right|_{\psi=\psi_o}$ , $p^2 = \frac{l^2\pi^2}{I}$. $\qquad$ (III.2.5)

If $g_1 < 0$ all eigenvalues $\mu(l)$ are real and the largest eigenvalue is positive. Above all, this largest eigenvalue is monotone increasing in l. Therefore, the linear stability analysis predicts the growth of a spatial structure if $\psi_o > \psi_c$ but with an evolution according to the smallest possible wavelenght in the case of an initial homogeneous structure randomly disturbed.

III.2.3. Numerical simulations.

The partial differential equations (III.2.4) with the boundary conditions are approximated by finite difference schemes. The value of the parameter $\psi_c$ is taken 0.25. The initial value $\psi_o$ of $\psi$ is 1.0 and $\beta = 0.01$.

In the first reported simulation, this initial value is randomly disturbed. The first evolution gives the degenerate pattern of alternating maxima and minima as the linear analysis predicts. Further growth leads to competition between the growing centres and gives the pattern as depicted in figure (3.2.1): dotted line gives pattern at time 100h (h is gridspacing); continuous curve at time 1000h . All maxima in the $\psi$-pattern go along with minima in the $\sigma$-pattern. It is to be noted that the peakes in figure (3.2.1) are at single gridpoints at the final stages of the evolution, so the final pattern is rather degenerated.

The same sort of evolution is observed in the following simulations. Parameters and initial values are the same as above but now only the values of the four leftest gridpoints are disturbed with the same positive value. As the initial bump grows, a depletion zone is formed. In figure (3.2.2) the dotted line gives the pattern at time 500h. In Feeney e.a. [2] is reported that for $0.01 \leq \beta \leq 100$ the second maximum has an almost constant distance $\xi \approx 2.7$ from the original bump. In our simulations we have found that this distance is decreasing in $\beta$. (For $\beta = 0.01$, $\xi \approx 2.7$; $\beta = 0.1$, $\xi \approx 2.3$ and for $\beta = 1.0$, $\xi \approx 1.8$). As in figure (3.2.1) we see the breaking up of the blocklike structure in finer peakes. The final pattern degenerates to single gridpoint maxima.

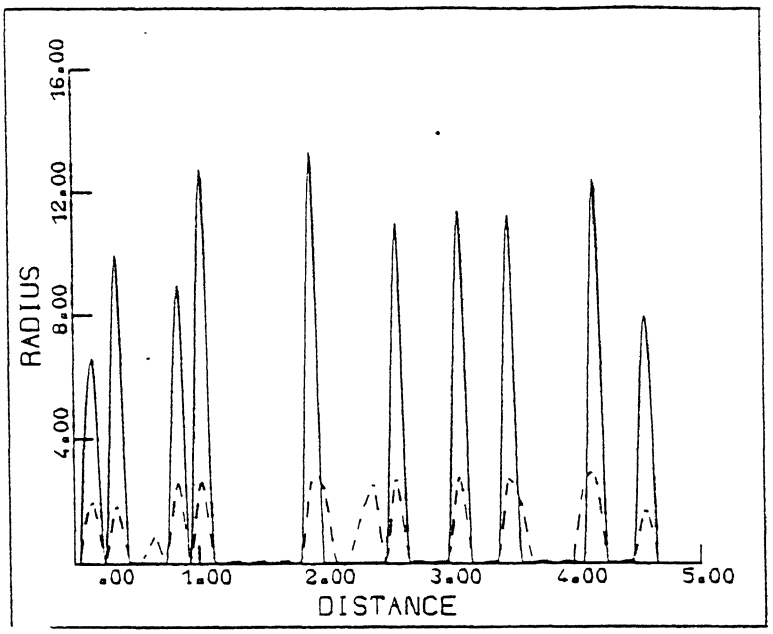


Figure 3.2.1: Competitive Particle Growth Model.

Initial homogenous state: randomly disturbed. $\beta$ = 0.01

--- : time= $100h^2$; —— : time= $1000h^2$, h is gridspacing.

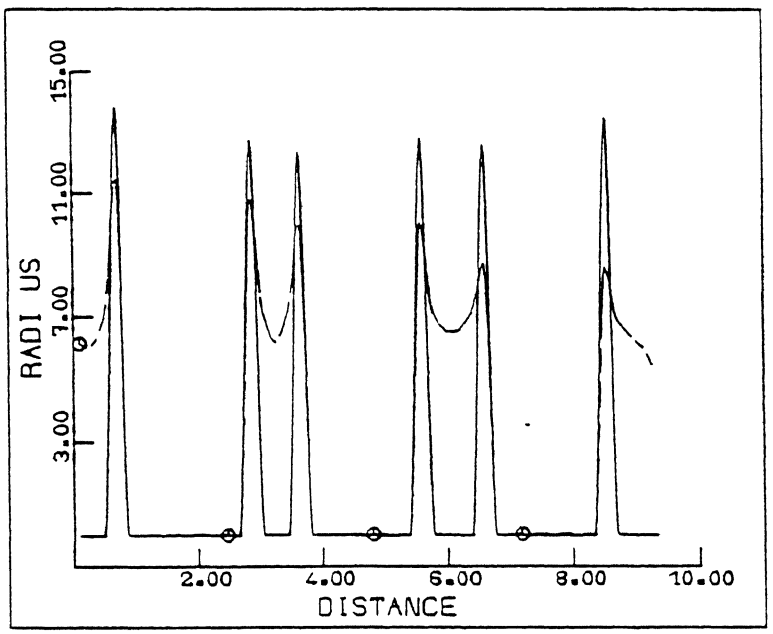


Figure 3.2.2: Competitive Particle Growth Model.

Initial homogeneous state only disturbed in the four left gridpoints. $\beta$ = 0.01

--- : time=$500h^2$; —— : time=$1000h^2$.

III.2.4. Comment.

Since R is taken to be greater then $R_c$, the model describes the evolution after the particles have reached at least a considerable size $R_c$. In making the assumption on the peaked particle-size distribution plausible, Feeney e.a. use the ripining process and state that such a distribution will be valid in the post nucleation regime. So accordingly, we interprete the equations as rather modelling phenomena such as secondary banding then as modelling the initial transient behavior in a Liesegang experiment. This means that the simulations here reported and in Feeney, in itself are simulations of the secondary banding process and not the *final* breakup in finer peaks as stated by Feeney e.a. [2]. Above all, this final breakup can be avoided by taken the function $C^{eq}(R)$, the equilibrium concentration, cubic in R with two stable branches, see (III.2.3).(figure 3.2.3).

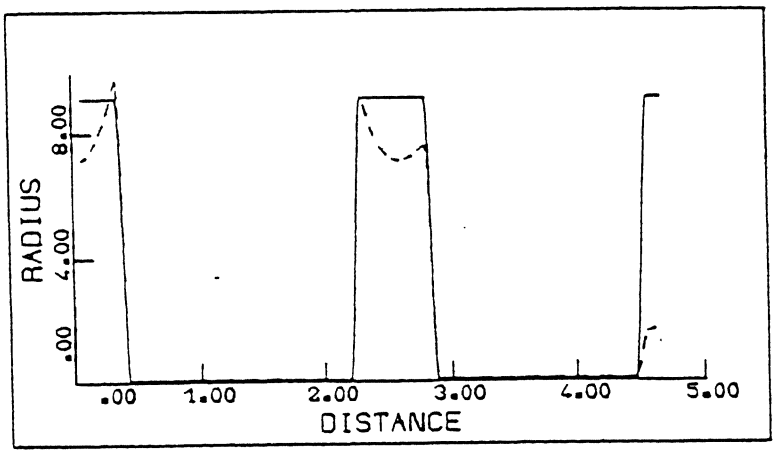


Figure 3.2.3: Competitive Particle Growth Model.
Equilibrium concentration function (III.2.3) with two stable branches. $\beta$ = 0.01
--- : time=500$h^2$; —— : time=1000$h^2$.

## III.3. An Anti-Diffusion Model.

The experiments (section II) have shown that ringformation depends about all on two environmental parameters: temperature and pH. Thermal fluctuations will cause deviations in the distributions of the components; at sufficiently high temperature such deviations are strong enough to form the germs of ringformation. At some particular pH level these germs are sustained and enhanced by a mass flow directed towards these local maxima in the Co density. Such a mass flow is best described as anti-diffusion as the direction is opposed to the standard linear Fickian diffusion mass flow. With sufficiently effective competition this mass flow causes a decomposition of the Co mass in regios with a low density and with a high density. Note that here only the early stages of ringformation are considered: small $Co[OH]_2$ clusters have a equilibrium concentration of the constituents which is a monotonically *increasing* function of the clustersize. So in high density areas the clusters can growth whereas in the low density areas the clusters dissolve. It is to be mentioned that such a diffusional clustering mechanism is reported also to be found in the so called spinodal alloys (e.g. [1]). In the spinodal regime the homogeneous state is unstable; every small fluctuation will initiate a decomposition of the conserved quantity.

In the following model the main aspect is the anti-diffusion term incorporated in the Co evolution equation; temperature effects are neglected and the role of the pH is modelled by making the anti-diffusion mechanism dependent of a second component simulating the OH-component of the system.

### III.3.1. Assumptions and model formulation.

A three component system is considered.

Assumptions :

i) As in section III.2, a multiple step chemical reaction is reduced to the following scheme :

$$A + 2B \underset{k_1}{\overset{k_{-1}}{\rightleftharpoons}} C \qquad \text{(III.3.1)}$$

where A is positive ion ($Co^{++}$), B a negative ion ($OH^-$) and C is an aggregate of AB molecules ( $Co[OH]_2$); $k_{-1}$, $k_1$ are postive reaction constants.

ii) For each cluster of $Co[OH]_2$ there exists an $Co^{++}$ equilibrium concentration $Co^{eq}$, but now small clusters are assumed such that $Co^{eq}$ is a monotone increasing function of the relevant cluster size.

This last assumption is consistent with the first evolution phase and is in contrast with assumption iii) of section (III.2.1). In our case a local maximum of the cluster size will only grow if, at least, the equilibrium between cluster size and $Co^{++}$ concentration can be restored by a flux of $Co^{++}$. Otherwise dissolution will occur. So, whereas in the competitive particle growth model an excess of Co (in that model rather $Co[OH]_2$) will diminish the clusters, the reverse is true in our model.

iii) A flux of Co towards a local maximum of the Co concentration, which goes along with a local maximum in the cluster size by assumption ii), is only possible beyond some level $B_c$ of the negative ion ($OH^-$) concentration. (We shall take this threshold constant but a temperature dependence is possible.)

In the formulation of our model we concentrate on a growth mechanism of $Co[OH]_2$ amplified by an aggregating process of the Co-component. So, rather than modelling the evolution of the clustersize, we shall model the evolution of $Co[OH]_2$ concentration itself. In that sense assumption ii) is interpretated.

The aggregating process of the Co-component is seen as a

diffusion like mass transport process which, for sufficient high $OH^-$ concentration, will be directed towards local maxima of the Co-concentration. The time evolution of such a process for a density u is governed by an "anti-diffusion" equation and has the following basic form :

$$\frac{\partial u}{\partial t} = \Delta \left[ \phi(u) - \varepsilon \Delta u \right] \qquad \text{(III.3.2)}$$

where $\Delta$: Laplacian operator, $\phi(u)$ is cubic in u with $\frac{\delta \phi}{\delta u}\Big|_{u=0} < 0$ and $\varepsilon > 0$. The name "anti-diffusion" becomes clear by neglecting all higher then first order terms in u: the right hand side of (III.3.2) holds a pure diffusion term with negative coefficient. This equation is derived in [4] without the use of potential functions by directly describing the dynamics of the distribution of watersheds in the context of Thom's river basin model. It was also shown that the evolution is governed by a Lyapunov functional which has surprisingly the same form as the well known Landau-Ginzburg functional. In [5] it is shown that equation (III.3.2) is the most probable evolution path equation for u if u is a conserved quanity, the time evolution of u is a stochastic process and the probability distribution of u is given by some non-stationary Markov process. In the form here used transitions in u are restricted to diffusion (mass transport) like changes. The probability of these changes is governed by the Lyapunov functional c.q. Landau-Ginzburg functional ( see below). The relation between (III.3.2) and this free energy functional can be made explicit in the following way.
Let the free energy functional V(u) be given by :

$$V(u) = \int f(u) + 0.5\, \varepsilon\, (\nabla u)^2 \, dx \qquad \text{(III.3.3)}$$

then $\phi(u) - \varepsilon \Delta u = \frac{\delta V}{\delta u}$ if $f(u) = \int \phi(s) ds$.

f(u) is to be interpretated as the free energy density function for a homogeneous system whereas the term $\varepsilon(\nabla u)^2$ ($\varepsilon>0$) takes account of the non-uniform environment of cell elements in a system with large concentration gradients (gradient energy), see

Cahn who used the same form of equation in describing phase transitions at the spinodal [1].
Let us assume $\phi(u)$ is given by :

$$\phi(u) = r_0 u - r_1 u^2 + r_2 u^3 \ , \text{ with } r_2 > 0 \qquad \text{(III.3.4)}$$

In general $r_0$ depends on an environmental parameter such as temperature or in this case, the pH of the system. Now, if $r_0$ becomes negative and $\varepsilon$ is small enough, the constant solution $u \equiv 0$ of (III.3.3) becomes unstable. The final patterns generated by (III.3.3) are bounded non-constant solutions; otherwise stated, the spatial domain becomes divided in aggregated and non-aggregated areas. Note that (III.3.3) with (III.3.4) models a second order phase transition with mass conservation in the u variable. In our model we shall incorporate this equation with $r_0$ depending on the OH concentration.

The dissolution and the precipitation effect on the growth of $Co[OH]_2$ clusters will be approximated by the chemical reaction scheme (III.3.1). Of course, this reaction is the growth source of $Co[OH]_2$ but the pattern generating process can only be inititated and sustain by a sufficient strong aggregating mechanism in the Co-component; and the effectivity of this process will be diminished by depletion of Co through the reaction mechanism. For instance, the role of $NH_4Cl$ in the pattern formation process can be simulated by changing the reaction constants $k_1$ and $k_{-1}$ in (III.3.1).

Finally, only standard, Fickian diffusion is assumed to be valid for the OH component since the experiments have not given any evidence that the OH-diffusion is affected by ringformation.

Then the following model is derived , with $A = [Co^{++}]$, $B = [OH^-]$ and $C = [Co[OH]_2]$:

$$\frac{\partial A}{\partial t} = -k_1 AB^2 + k_{-1} C + D_A \Delta \left[ \psi(A,B) - E_A \Delta A \right] \qquad \text{(III.3.5.1)}$$

$$\frac{\partial B}{\partial t} = -2k_1AB^2 + 2k_{-1}C + D_B \Delta B \qquad \text{(III.3.5.2)}$$

$$\frac{\partial C}{\partial t} = k_{-1}C - k_1AB^2 \qquad \text{(III.3.5.3)}$$

where $D_A$, $D_B$ are positive diffusion constants,
$\psi(A,B) = (-B + B_c)A - r_1A^2 + r_2A^3$ with $r_2 > 0$.
with $B_c$ some positive constant reflecting pH-dependence of aggregation of the Co-component. The anit-diffusion term is the third term in the right hand side of (III.3.5.1). $E_A$ is positive constant.
Let $A = A_o(1 + \alpha)$, $B = B_o(1 + \beta)$ and $C = C_o(1 + \gamma)$ such that $k_{-1}C_o = k_1A_oB_o$; let $\bar{t}$ and $\bar{L}$ be time- and space scaling factors such that $\frac{D_A\,\bar{t}}{\bar{L}^2} = 1$ then equations (III.3.5) reduce for a one dimensional spatial domain $[\,0,\ L\,] \subset \mathbb{R}$ to:

$$\frac{\partial \alpha}{\partial \tau} = -k\left[(1 + \alpha)(1 + \beta)^2 - (1 + \gamma)\right] + \frac{\partial^2}{\partial \xi^2}\left[\phi(\alpha,\beta) - \varepsilon \frac{\partial^2 \alpha}{\partial \xi^2}\right] \qquad \text{(III.3.6.1)}$$

$$\frac{\partial \beta}{\partial \tau} = -2k\left[(1 + \alpha)(1 + \beta)^2 - (1 + \gamma)\right] + D_\beta \frac{\partial^2 \beta}{\partial \xi^2} \qquad \text{(III.3.6.2)}$$

$$\frac{\partial \gamma}{\partial \tau} = -k\left[(1 + \gamma) - (1 + \alpha)(1 + \beta)^2\right] \qquad \text{(III.3.6.3)}$$

where, for simplicity, is taken $A_o = B_o = C_o$, $k = k_1B_o^2$ and

$$\phi(\alpha,\beta) = (-\beta + \beta_c)\alpha - r_1'\alpha^2 + r_2'\alpha^3 \text{ with } r_2' > 0 \qquad \text{(III.3.6.4)}$$

In the following $r_1' = 1$, $r_2' = 1$ are taken.
No-flux boundary conditions are assumed.

## III.3.2 Linear stability analysis.

For the homogeneous solution $(\alpha,\beta,\gamma) \equiv (0,0,0)$ the evolution equations for the disturbances u of $\alpha \equiv 0$, v of $\beta \equiv 0$ and w of $\gamma \equiv 0$ are given in linear approximation by :

$$\frac{\partial u}{\partial \tau} = -k(u+ 2v - w) + \beta_c \frac{\partial^2 u}{\partial \xi^2} - \varepsilon \frac{\partial^4 u}{\partial \xi^4} \qquad \text{(III.3.7.1)}$$

$$\frac{\partial v}{\partial \tau} = -2k(u + 2v - w) + D_\beta \frac{\partial^2 v}{\partial \xi^2} \qquad \text{(III.3.7.2)}$$

$$\frac{\partial w}{\partial \tau} = k(u + 2v - w) \qquad \text{(III.3.7.3)}$$

Given the no-flux boundary conditions the eigenvectors of this linear system are proportional to $\cos(\frac{l\pi\xi}{L})$, $l = 0,1,2,..$ and the eigenvalues $\mu(l)$ must satisfy :

$$\mu^3(l) + \mu^2(l)\left\{\varepsilon p^4 + D_\beta p^2 + \beta_c p^2 + 6k\right\} + \mu(l)\left\{\varepsilon D_\beta p^6 + \right.$$

$$\left. + (5\varepsilon k + D_\beta\beta_c)p^4 + (2kD_\beta + 5k\beta_c)p^2\right\} + k(\varepsilon D_\beta p^6 + \beta_c D_\beta p^4) = 0$$

where $p^2 = \frac{l^2\pi^2}{L^2}$ . (III.3.8)

Then for $\beta_c > 0$ all eigenvalues are negative and the state $(\alpha,\beta,\gamma) = (0,0,0)$ is stable.

For $\beta_c < 0$ the system can become unstable; let $\beta_c = -0.1$, $\varepsilon = 0.0004$, $k = 0.1$ and $D_\beta = 5.0$ then the eigenvalues are positive for $0 \le l \le 23$ with maximal eigenvalue for $l = 17$. So, with a randomly disturbed initial state $(\alpha,\beta,\gamma)\equiv(0,0,0)$ the time evolution will be, at least in the early stages, according to a wavelenght corresponding with the maximal eigenvalue for $l = 17$.

A non-homogenous solution of (III.3.6) can be constructed by using the existence of non-constant bounded stable solution of the one dimensional anti-diffusion equation [4]:

$$\frac{\partial u}{\partial t} = \frac{\partial^2}{\partial \xi^2}\phi(u) - \varepsilon \frac{\partial^4 u}{\partial \xi^4} \quad , \ \varepsilon > 0 \qquad \text{(III.3.9)}$$

with $\phi(u) = -u + r_1u^2 + r_2u^3$ , $r_2 > 0$.

Such non-constant solutions do exist if the null solution $u\equiv0$ is unstable: Let $\beta(\xi) = \beta_o$, constant such that $\alpha\equiv0$ is an unstable solution of:

$$\frac{\partial \alpha}{\partial \tau} = \frac{\partial^2}{\partial \xi^2}\left[\phi(a,b_o) - \varepsilon \frac{\partial^2 \alpha}{\partial \xi^2}\right] \qquad \text{(III.3.10)}$$

with $\phi$ as defined in (III.3.6.4).
Then there exists a non-constant stable bounded solution $\alpha(\xi)$ of (III.3.10), see [4]. Take $\gamma(\xi)$ such that:

$$\gamma(\xi) = (1 + \beta_o)^2(1 + \alpha(\xi)) - 1 \quad , \forall\ \xi \in [0,L] \qquad \text{(III.3.11)}$$

then $(\alpha(\xi),\beta_o,\gamma(\xi))$ is a stationair solution of (III.3.6).

If the evolution of $\beta(\xi)$ is neglected, that is $\beta(\xi) = 0$ for all $\xi$ and all time t and the system is reduced to the equations (III.3.6.1) and (III.3.6.3), such a solution will be stable. Since $\alpha(\xi)$ is a stable solution of (III.3.10) the equation obtained by linearizing (III.3.10) in $\alpha(\xi)$ will have a complete set of eigenvectors $W_\alpha(\xi)$ with all eigenvalues equal or less than zero. The reaction terms in (III.3.6.1) and (III.3.6.3) are linear in $\alpha$ and $\gamma$, and stable, so the linear system obtained by linearising (III.3.6.1) and (III.3.6.3) in $(\alpha(\xi),\gamma(\xi))$ is a stable system and all disturbances as expressed in terms of the eigenvectors $W_\alpha(\xi)$ will be damped.

## III.3.3. Numerical simulations.

The numerical simulations can be divided in two sections.
First: the initial homogeneous state $(\alpha,\beta,\gamma)\equiv(0,0,0)$ is randomly disturbed. If $\beta_c$ is positive no pattern formation occurs.
For $k = 0.1$, $D_\beta = 5$, $\beta_c = -0.1$ and $\varepsilon = 0.0004$ the null solution is unstable. Figure 3.3.1 gives the final pattern; not shown is the $\beta$-component which becomes homogeneous with $\beta = 0.05$ which is sufficiently high to let the null solution unstable ( $\beta_c = -0.1$). So the final pattern is indeed of the form as given in the second part of the foregoing section.
Note that based on the linear stability analysis an evolution pattern with wavelenght (2L/9) was to be expected; in this case the final pattern has approximately this wavelenght.

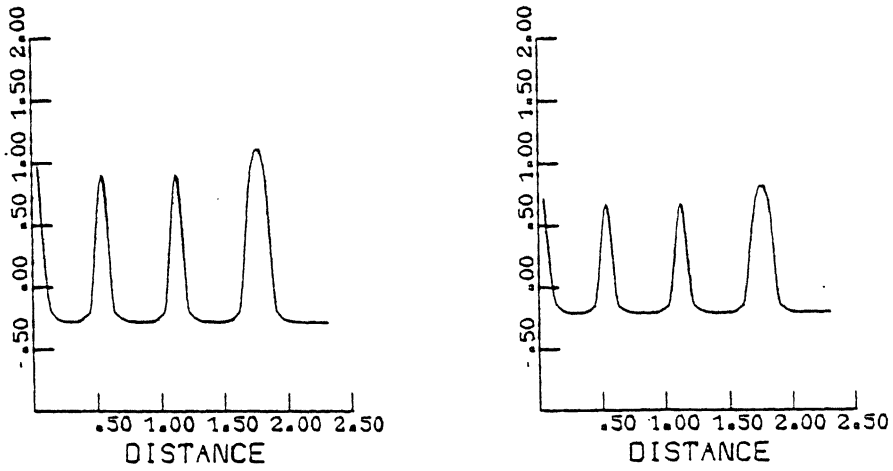


Figure 3.3.1: Anti-diffusion Model.
Final pattern; initial state: homogeneous, randomly disturbed. (k=0.1; $\beta$=-0.1; D=5.0; $\varepsilon$=0.0004)
left figure: $\alpha$ pattern; right figure: $\gamma$ pattern.

In the second group of simulations the parameters are taken such that now the null solution $(\alpha,\beta,\gamma)\equiv(0,0,0)$ is stable. Now a pattern generating evolution is inititated by a large bump of the $\beta$-component on the left side of the grid. (This can be seen as an approximation of the experiments with homogeneous distributed $Co^{++}$ and an $OH^-$-injection in the centre of the system, see section II.) For all reported simulations holds that $\beta_c = 0.01$, $D_\beta = 5.0$ and $\varepsilon = 0.0004$.

The patterns depicted in figure 3.3.2 are generated with k = 0.1 and those of figure 3.3.3 with k = 1.0. In both cases the final pattern of $\beta$ is an homogeneous one with a value sufficiently high to make the null solution unstable. The role of the reaction term as simulating dissolution effects is obvious; if k is taken to be 100 we don't get any pattern at all and the final state was an homogeneous one with (stable) non-zero solutions. If the initial bump in the $\beta$-component is too small the final state is also an homogeneous one.

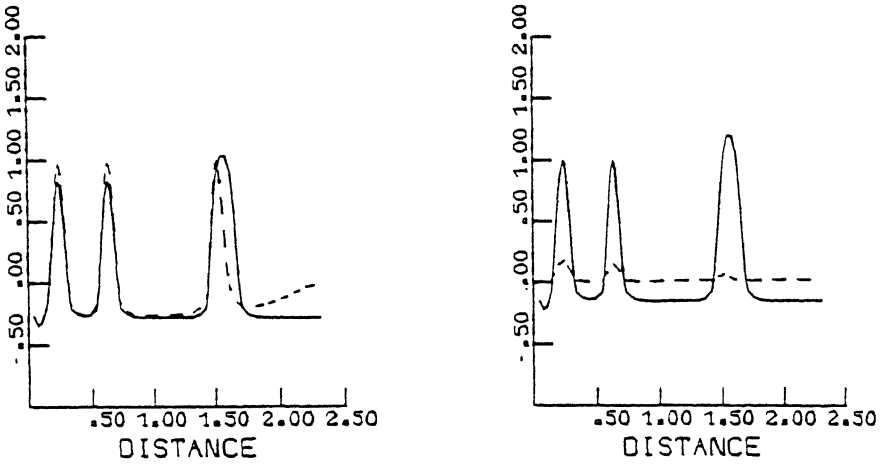


Figure 3.3.2: Anti-diffusion Model.

Final patterns after disturbing an initial homogeneous state with a large bump of $\beta$ at the left side.
left: $\alpha$ evolution; right: $\gamma$ evolution; $\beta$ final:homogeneous.
--- : time $50h^2$; —— : time $1000h^2$; (h: gridspacing).
($k=0.1$; $\beta_c=0.01$; $D_\beta=5.0$; $\varepsilon=0.0004$).

---

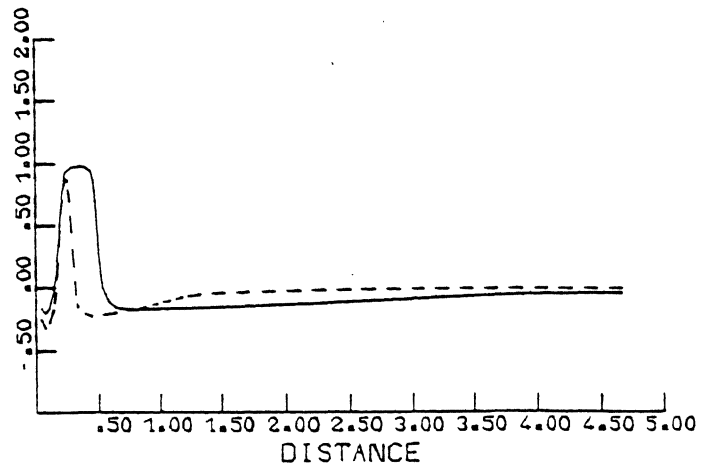


Figure 3.3.3: Anti-diffusion Model.

The same initial values and parameters as in figure 3.3.2 except for k; k = 1.0;
Only $\alpha$-patternis hown. $\gamma$:similar to $\alpha$; $\beta$ homogeneous.--- : time $50h^2$; —— : time $1000h^2$; (h:gridspacing).

III.3.4. Comment.

The model named as anti-diffusion has two major features : aggregation instability depending on the $\beta$-component ($OH^-$-concentration) and dissolution stability. Both aspects are consistent with the observations reported in section II. The introduction of an anti-diffusion term seems phenomenological based but is in agreement with phase transition models based on the Landau-Ginzburg free energy functional. The anti-diffusion model is only a particular form of models based on the Landau-Ginzburg functional: one with mass conservation.

Till now we don't make any attempt to predict the final state generated by this model in the sense of distances between or the size of the concentration centres e.a. since calculations based on linear approximation and the subsequently calculated fastest growing mode, can only have minor prediction power as numerical simulations of the basic model (III.3.2) have shown [4]. But the model is capable in simulating many of the aspects of a Liesegang experiment as ringformation dependence on pH, $NH_4Cl$ effects and size of the OH "injection".

## IV. Conclusions.

In this concluding remarks we summarize the main construction principles and assumptions of the models reviewed in this paper.

The autocatalytic growth model is based on a supplementary growth mechanism induced by supposed electric double layer effects. This process is modelled by an autocatalytic reaction scheme. However, electric double layers are rather stabilising a sol then the source of instability which is confirmed by the ringformation dependence on the $NH_4Cl$ concentration.

The competitive particle growth model is based on a competition between particle growth and dissolution in a state where the equilibrium concentration for a particle (polymer) and

LIST OF REPORTS 1987

8700 Publications of the Econometric Institute Second Half 1986: List of Reprints 458-469.

8701/A **J. van Daal and D.A. Walker**, "The problem of aggregation in Walrasian general equilibrium theory", 23 pages

8702/A **L. de Haan and I. Weissman**, "The index of the outstanding observation among n independent ones", 15 pages.

8703/B **H. Bart and H. Hoogland**, "Complementary triangular forms of pairs of matrices, realizations with prescribed main matrices, and complete factorization of rational matrix functions", 48 pages.

8704/A **H.K. van Dijk**, "Some advances in Bayesian estimation methods using Monte Carlo integration", 48 pages.

8705/A **B.M.S. van Praag and J.P. Hop**, "Estimation of continuous models on the basis of set-valued observations", 34 pages.

8706/A **J. Csirik, J.B.G. Frenk, G. Galambos and A.H.G. Rinnooy Kan**, "Probabilistic analysis of algorithms for dual bin packing problems", 16 pages.

8707/C **R. de Zwart en E. de Vries**, "Van kinderbijslag naar basisbeurs; effecten van een nieuwe wet", 49 pagina's.

8708/B **R.J. Stroeker and N. Tzanakis**, "On the application of Skolem's p-adic method to the solution of Thue equations", 30 pages.

8709/A **M. Meanti, A.H.G. Rinnooy Kan, L. Stougie and C. Vercellis**, "A probabilistic analysis of the multiknapsack value function", 10 pages.

8710/A **L. de Haan and S. Resnick**, "On regular variation of probability densities", 15 pages.

8711/B **H. Bart and P.S.M. Kop Jansen**, "Upper triangularization of matrices by lower triangular similarities", 28 pages.

8712/A **J. van Dalen, J. Koerts and A.R. Thurik**, "The analysis of demand and supply factors in retailing using a disequilibrium model", 20 pages.